 n information: DOI 10.1109/TMECH.2018.2817246, IEEE/ASME

Sensorless PMSM Drive Based on Stator Feedforward Voltage Estimation Improved With MRAS Multi-Parameter Estimation

Omer Cihan Kivanc, *Member*, *IEEE*, Salih Baris Ozturk, *Member*, *IEEE*

***Abstract*— In order to reduce the adverse effect of parameter variation in position sensorless speed control of permanent magnet synchronous motor (PMSM) based on stator feedforward voltage estimation (FFVE), multi-parameter estimation using model reference adaptive system (MRAS) is proposed. Since the FFVE scheme relies on motor parameters, the stator resistance and rotor flux linkage are estimated and continuously updated in the feedforward voltage estimation model in a closed-loop fashion, sensitivity to multi-parameter changes at low speed is eliminated. To improve the dynamics and stability of the overall system and eliminate transient oscillations in speed estimation, a PLL-like speed estimation method is proposed which is obtained by passing the q–axis PI current regulator output through a first order filter in the FFVE scheme. The proposed control method is similar to V/f control as in induction motors, therefore starting from zero speed is possible. The experimental tests are implemented with 1 kW PMSM drive controlled by a TMS320F28335 DSP. The proposed sensorless scheme is also compared with the classical Sliding Mode Observer (SMO). Experimental results show that the proposed sensorless scheme exhibits greater stability at lower speed than the classical SMO under parameter detuning. Experimental results and stability analysis demonstrate the feasibility and effectiveness of the proposed sensorless scheme for PMSM under various load and speed conditions.**

***Index Terms*—Permanent magnet synchronous motor (PMSM), model reference adaptive system (MRAS), sensorless control, stator feedforward voltage estimation (FFVE), Volt/Hz control, V/f control, V/Hz control, parameter estimation, parameter detuning, parameter variation, multi-parameter estimation.**

I. Introduction

Permanent magnet synchronous motor (PMSM) drives have been extensively used in many applications, ranging from servo to traction drives due to several distinct advantages such as high power density, robustness, high efficiency, large torque to inertia ratio and better controllability [1]–[3].

In the majority of the back-EMF based sensorless control methods, the PMSM steady-state model is taken as a reference, therefore stability cannot be achieved when mismatches of parameters and variation of loading conditions occur during operation in the zero to low speed region [4], [5]. Since stator resistance and rotor flux linkage vary due to temperature variation, magnetic saturation and aging, robust and accurate multi-parameter parameter estimation is inevitably required for sensorless drives to operate at low speeds [1], [5], [6]. In order to minimize the effects of these changes and to accurately tune the control parameters correctly, several online parameter estimation methods using extended Kalman filter (EKF) [7], [8], recursive least squares (RLS) [9], [10], artificial neural network (ANN) [11], full-order observers [12], reduced-order observers [13], and model reference adaptive system (MRAS) [14]–[17] have been introduced for PMSM drives in recent work.

In [7], the EKF method gives suitable results in rotor flux estimation, however it has the disadvantages of complex algorithmic structure, the challenges of parameter adaptation, proper initialization, and insensitivity to noise. The recursive least square (RLS) method suggested in [9] and [10] for the estimation of electrical parameters provides fast convergence rate, however due to the mass of differential expressions, it reduces the performance of the microprocessor and causes the system to respond slowly. In [11], an ANN based rotor flux estimation method is proposed which contains excessive amount of mathematical calculations, therefore its applications to industrial drives is difficult. In [12], stator flux is estimated using a full-order observer. Although it is a robust estimation method, the accuracy of the full-order observer still depends on the other motor parameters. Moreover, the design of the observer gain matrix is quite complicated. In [13], the reduced-order rotor flux observer is proposed in which the mechanical parameters are removed in the observer design. The current values from sensors can be distorted by noise and disturbance. Therefore, the reduced-order flux observer can generate distortion in the estimated parameters. The model reference adaptive system (MRAS) is proposed in [18] and [19] in which stator resistance and rotor flux are continuously estimated. Although, accurate simultaneous estimation of three motor parameters (winding resistance, inductance and rotor flux linkage) is not possible, due to less computational requirements and rapid response, compared to other techniques model reference adaptive system (MRAS) for PMSM drives is one of the most promising parameter estimation methods.

More recently, due to fast convergence speed, the particle swarm optimization (PSO) methods presented in [20], [21] have been an attractive optimization technique in PMSM

This work was supported by The Scientific and Technological Research Council of Turkey (TUBITAK) funded project (112E263).

O. C. Kivanc and S. B. Ozturk are with the Department of Electrical and Electronics Engineering, Okan University, Tuzla, Istanbul 34959, Turkey (e-mail: cihan.kivanc@okan.edu.tr; baris.ozturk@okan.edu.tr).

n information: DOI 10.1109/TMECH.2018.2817246, IEEE/ASME

parameter estimation. However, PSO methods developed for steady-state operation may not be applicable to machines under dynamic operating conditions such as load disturbance and speed variations. Online multi-parameter identification of surface-mounted PMSM under maximum torque per ampere (MTPA) control considering inverter disturbance voltage is suggested in [22] where three motor parameters (winding resistance, inductance, and rotor flux) are estimated. To improve the estimation accuracy of the method incorporating offline and online voltage source inverter (VSI) disturbance voltage estimation, both independent of motor parameters and switching device parameters are combined with the d–axis current injection method. Due to the use of multiple methods, the system becomes complicated. Moreover, signal injection is used in the estimation process, therefore acoustic noise is inevitable. In [23], the proposed multi-parameter estimation method is composed of two affine projection algorithms (APA), one for dq–axes stator inductances and the other for stator resistance, rotor flux linkage and load torque. Then, they are incorporated into the adaptive decoupling PI controllers with MTPA operation for interior PMSM drive, therefore better steady-state and transient performances are achieved, however the method requires gain retuning under speed changes due to mechanical parameter uncertainties. Moreover, the discretization error and the solution for the discretization problem are not provided. An adaptive interconnected observer in the stationary reference frame has recently been proposed in [24] for the sensorless control of a PM motor to estimate the stator inductance, stator resistance and load torque, simultaneously. The parameters are estimated accurately, but the proposed method has poor robustness when dealing with the uncertainties in the estimation of machine parameters. In [25] and [26], the current signal injection and the RLS algorithm are utilized to estimate d– and q–axes inductances, stator resistance and flux linkage, simultaneously. In [27] and [28], the d– and q–axes current injection technique is proposed during the steady state. It is assumed that the change of dq–axes inductances are linear to their corresponding dq–axes currents. In order to obtain the d– and q–axes inductances on-line, the RLS algorithm is utilized to solve the steady state machine equations. However, RLS and APA based methods require considerable amount of convergence time and tuning the parameters is not straightforward. Conventional parameter estimations methods may be insufficient for multi-phase machines, therefore a detailed machine model is suggested in the literature, for example, a new six-phase machines vector space decomposition (VSD) model has been proposed in [29]. In addition, estimation design with sliding-mode observer (SMO) techniques has been extensively investigated in the literature with respect to various types of systems, for example, Markovian jump systems [30]. An adaptive parameter estimation that are modified via a sliding mode technique to achieve finite-time convergence, and an online verification of the alternative persistent excitation (PE) condition and control for nonlinear robotic systems based on parameter estimation errors are introduced in [31]. Moreover, state and fault estimation problems for continuous-time switched systems with simultaneous disturbances, sensor and actuator faults are solved by two types of observers in [32].

In summary, parameter estimation methods are required not only for condition monitoring and fault diagnosis, but they are also widely used for sensorless ac drives to enhance the wide speed performance. It is well-known that the back-EMF based sensorless estimation methods are heavily affected by the parameter variation. In this paper, multiple parameter estimation based on MRAS is incorporated with the sensorless feedforward voltage estimation (FFVE) for PMSM drive. FFVE method is first introduced for IM in [33], [34] as a back-EMF based sensorless speed control strategy with performance lies between V/Hz control and indirect field-oriented control (IFOC) [35]. The performance of IM with respect to stator resistance variation have been investigated in [35]. In [36], [37], the stator resistance is adjusted based on the d–axis current error, therefore the low frequency operation of sensorless IM drive is feasible [35]. In [38], FFVE based sensorless PMSM drive with a novel Luenberger rotor flux linkage observer has been developed. Since the stator resistance which is a crucial parameter in low speed operation is not estimated, the sensorless scheme fails at low speed. Although the Luenberger observer is used in [38] which is robust and reliable, the higher number of observer gains are required especially for multiple parameter estimations as oppose to a more simpler MRAS estimator which has an adaptive correction mechanism with less amount of gain requirements.

The main contribution of this paper is to improve the low speed performance of the feedforward voltage estimation (FFVE) based speed sensorless control scheme for PMSM drive incorporating mathematically modified MRAS estimator to continuously estimate the stator resistance and rotor flux linkage magnitude, while stator inductance is set to its nominal value. The updated values are used in the feedforward voltage estimation model in a closed-loop fashion. With the MRAS multi-parameter estimation, performance and stability of the sensorless drive scheme in steady state and in low speed are improved significantly. Experimental results demonstrate the feasibility and effectiveness of the proposed position sensorless method.

II. Details of the Proposed Sensorless PMSM Drive Based on Stator FFVE Using MRAS Multi-parameter Estimation

A. Dynamic and Steady-State Mathematical Model of PMSM

The dynamic dq model in the rotating synchronous reference frame is used to analyze the PMSM for the field-oriented control (FOC). The stator voltage equations of the PMSM in the rotating (rotor/synchronous) dq reference frame are given by (1) and (2), omitting the influences of magnetic field saturation and magnetic hysteresis as

$$v_q = i_q R_s + L_q \frac{di_q}{dt} + (\omega_e L_d i_d + \omega_e \lambda_f) \tag{1}$$

$$v_d = i_d R_s + L_d \frac{di_d}{dt} - \omega_e L_q i_q \tag{2}$$

n information: DOI 10.1109/TMECH.2018.2817246, IEEE/ASME

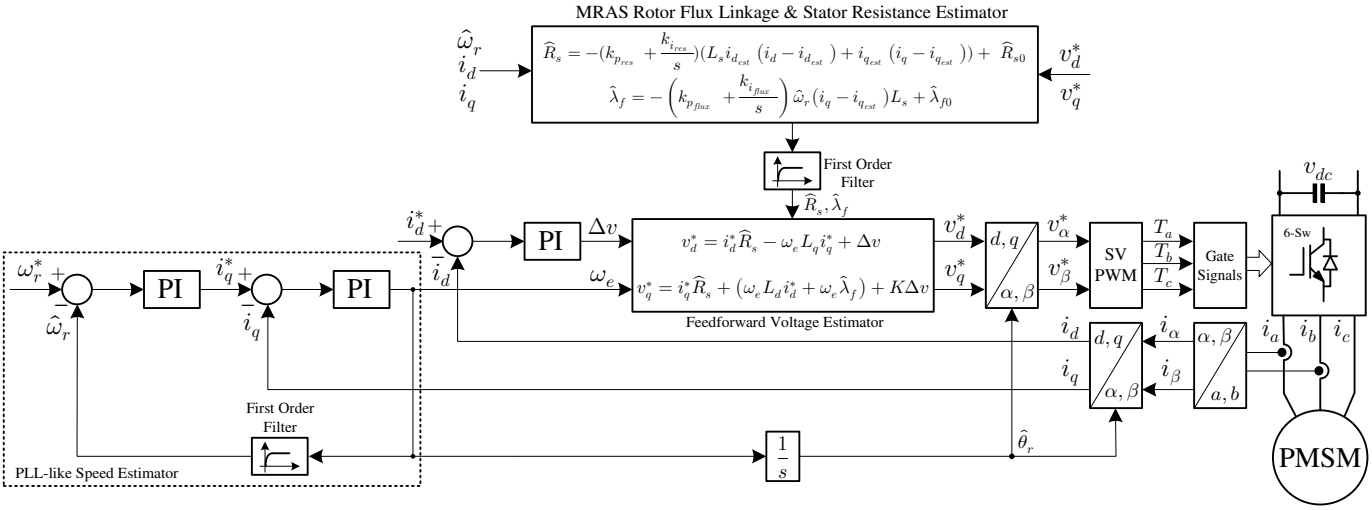

Fig. 1. Overall block diagram of the proposed speed sensorless PMSM drive model based on MRAS multi-parameter estimation.

where v_d, v_q, i_d, i_q are the stator d– and q–axes voltages and currents in the rotor reference frame, respectively; R_s is the stator winding resistance; L_d and L_q denote the d– and q–axes inductance, respectively; ω_e is the rotor angular electrical velocity; and λ_f is the flux linkage due to the permanent magnet rotor flux.

The steady state form of dq–axes stator voltage equations can be derived from (1) and (2) by making derivative terms equal to zero in each equation as

$$v_q = i_q R_s + (\omega_e L_d i_d + \omega_e \lambda_f) \tag{3}$$

$$v_d = i_d R_s - \omega_e L_q i_q. \tag{4}$$

B. Principles of Feedforward Stator Voltage Estimation

The dq–axes stator voltages in field oriented control are used in order to perform the current control located in the inner loop more dynamically [39]. In the literature, similar to the method proposed for induction motor sensorless speed control, stator voltage references v_d^* and v_q^* are added to the PMSM steady-state equation as feedforward estimator signals [33], [34], [36]. The dynamically enhanced modified feedforward stator dq–axes voltages that are derived from a steady-state PM synchronous machine model are applied to the PM motor. The dynamic resemblance of the actual PM machine is accomplished by the help of d*– and q*–axes PI regulator outputs which are composed as the components of the feedforward voltage models [37].

The derivative term in the voltage equations is represented by the output of the d–axis PI regulator, and the q–axis PI current regulator output with a simple filtering formulates the speed estimation algorithm. A complete block diagram representation for a field-oriented control of the proposed speed sensorless PMSM scheme based on feedforward stator voltage estimation with an MRAS multi-parameter estimation using a space vector PWM (SVPWM) VSI is illustrated in Fig. 1. The control principle is adopted where the current in the q–axis is controlled by speed of rotation or frequency of stator voltage applied to q–axis winding. The amplitude of the q–axis voltage is obtained by neglecting the derivative term and assuming that the real currents closely follow the reference values $i_q = i_q^*$ and $i_d = i_d^*$ (reference values are marked with * in the superscript and hat $\wedge$ is the symbol that indicates estimates). The modified feedforward stator voltage equations for the proposed speed sensorless scheme are given in dq reference frame as

$$v_q^* = i_q^* \widehat{R}_s + \left(\omega_e L_d i_d^* + \omega_e \hat{\lambda}_f\right) + K\Delta v \tag{5}$$

$$v_d^* = i_d^* \widehat{R}_s - \omega_e L_q i_q^* + \Delta v \tag{6}$$

where Δv is the output of the d–axis PI current regulator and ω_e is the electrical angular speed which is the output of the q–axis PI current regulator. Δv is multiplied by K gain and added to q–axis voltage equation v_q^* representing the part of the derivative term in the dynamic voltage equation given in (1). Similarly, the Δv term in (5) also acts as the derivative representation given in (2) to achieve a better transient response in the sensorless operation. Under dynamic conditions such as load disturbance, reference and parameter changes, a misalignment between the reference frame and the rotor flux vector produces non-zero terms represented by the derivative term in the d–axis voltage which is the output of the d–axis current regulator called Δv. Since the feedforward control of v_d^* is determined by (2) on the assumption of existing field alignment, such a misalignment causing deviation will generate a correcting signal from the i_d controller. This signal through a K gain affects the q–axis voltage v_q^* and, therefore i_q as well, causing the q–axis current regulator to accelerate or decelerate the reference frame to reconstruct the correct field orientation [40], [41] and, therefore the accurate rotor speed is obtained.

During steady-state operation, while d–axis current i_d minimizes the rotor flux linkage error, q–axis current i_q reference is obtained from the output of the speed regulator and controls the torque, indirectly. The rotor flux linkage is defined as proportional to the rate of change of i_q and it is adjusted to force the d–axis current equal to zero at steady-state [42], [43]. Thus, the actual dq–axes voltages are proportional to the reference dq–axes voltages. Similar to the method that is sug-

 n information: DOI 10.1109/TMECH.2018.2817246, IEEE/ASME

gested in [33] for induction motors, the relationships of the d–axis current regulator output Δv and rotor flux linkage $\hat{\lambda}_f$ are represented at steady-state when $i_d^* = 0$ using (1) as

$$\Delta v \approx \frac{\omega_e \hat{\lambda}_f}{K} \tag{7}$$

where at steady-state ω_e is constant, therefore the rotor flux linkage $\hat{\lambda}_f$ is proportional to Δv which is approximated as

$$\hat{\lambda}_f \approx \Delta v. \tag{8}$$

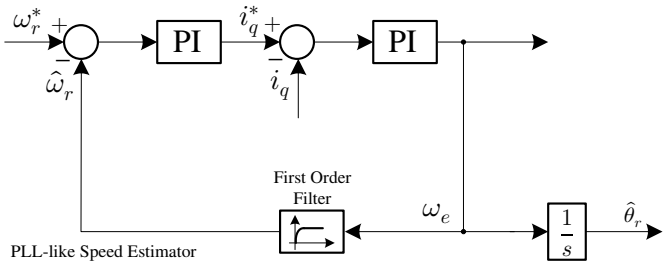

Fig. 2. PLL-like rotor speed and rotor angle estimation blocks.

The PLL type speed and position estimator is generally used to acquire the estimated rotor speed and position from the estimated rotor position error. In a similar fashion, in this study, the estimation of rotor speed $\hat{\omega}_r$ is obtained by passing the q–axis PI regulator output which constitutes the electrical angular speed ω_e through a first order low-pass filter resembling the closed-loop form of PLL, as shown in Fig. 2. The addition of the LPF in the PLL loop helps to improve the stability and mitigates the algebraic loop. The time constant of the filter depends on the overall system mechanical characteristics and heavily affects the dynamics and stability of the sensorless control scheme.

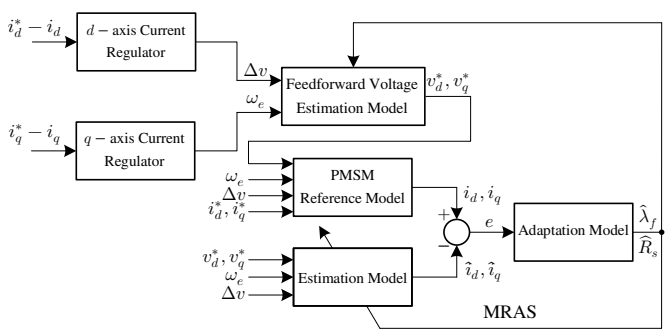

Fig. 3. Feedforward voltage estimation principle with MRAS multiple parameter estimation method.

C. Proposed Rotor Flux Linkage and Stator Resistance Estimator Based on Model Reference Adaptive System (MRAS)

In order to eliminate the errors caused from the stator resistance and rotor flux linkage variation in the sensorless PMSM drive, multi-parameter estimation using MRAS method is performed. MRAS parameter estimation equations are modified to be used in the proposed stator feedforward voltage estimation. PMSM reference frame and adjustable models that are given in (9) and (10), respectively are modified accordingly. The novel MRAS mathematical models are derived to be used in accordance with the feedforward voltage estimation model. The overall block diagram of the proposed MRAS parameter estimator model is shown in Fig. 3. The variables $K\Delta v$ and Δv in the reference model are added to construct the proposed steady-state PMSM equations. The modified MRAS equations consist of a feedforward linear model and a non–linear feedback component are expressed as

$$\begin{bmatrix} \frac{di_q}{dt} \\ \frac{di_d}{dt} \end{bmatrix} = \underbrace{\begin{bmatrix} -\frac{R_s}{L_q} & -\frac{L_d}{L_q}\omega_e \\ \frac{L_q}{L_d}\omega_e & -\frac{R_s}{L_d} \end{bmatrix}}_{A} \begin{bmatrix} i_q \\ i_d \end{bmatrix} + \underbrace{\begin{bmatrix} \frac{1}{L_q} & 0 \\ 0 & \frac{1}{L_d} \end{bmatrix}}_{B} \begin{bmatrix} v_q \\ v_d \end{bmatrix} + \underbrace{\begin{bmatrix} -\frac{\lambda_f}{L_q}\omega_e \\ 0 \end{bmatrix}}_{C} + \underbrace{\begin{bmatrix} -K\Delta v \\ -\Delta v \end{bmatrix}}_{E} \tag{9}$$

where $\widehat{R}_s$ and $\hat{\lambda}_f$ are the estimated stator resistance and rotor flux linkage, respectively which are the outputs of the adaptation model. $\widehat{R}_s$ and $\hat{\lambda}_f$ are updated in the estimation block in the closed loop system. As a result, the estimated currents $\hat{i}_q$ and $\hat{i}_d$ are obtained as

$$\begin{bmatrix} \frac{d\hat{i}_q}{dt} \\ \frac{d\hat{i}_d}{dt} \end{bmatrix} = \underbrace{\begin{bmatrix} -\frac{\widehat{R}_s}{L_q} & -\frac{L_d}{L_q}\omega_e \\ \frac{L_q}{L_d}\omega_e & -\frac{\widehat{R}_s}{L_d} \end{bmatrix}}_{\hat{A}} \begin{bmatrix} \hat{i}_q \\ \hat{i}_d \end{bmatrix} + \underbrace{\begin{bmatrix} \frac{1}{L_q} & 0 \\ 0 & \frac{1}{L_d} \end{bmatrix}}_{\widehat{B}} \begin{bmatrix} v_q \\ v_d \end{bmatrix} + \underbrace{\begin{bmatrix} -\frac{\hat{\lambda}_f}{L_q}\omega_e \\ 0 \end{bmatrix}}_{\hat{C}} + \underbrace{\begin{bmatrix} -K\Delta v \\ -\Delta v \end{bmatrix}}_{E} + \underbrace{\begin{bmatrix} G_1 & 0 \\ 0 & G_2 \end{bmatrix}}_{G} \begin{bmatrix} i_q - \hat{i}_q \\ i_d - \hat{i}_d \end{bmatrix} \tag{10}$$

where G is an observer gain matrix, G_1 and G_2 are coefficients of the G matrix which ensures that the feedforward linear model is positive and a real number. Selection of accurate values of G_1 and G_2 gains given in (10) eliminate the algebraic loop problems that occur in experimental studies. In order to obtain the desired poles of the current estimator model, the observer gain matrix G should consist of symmetric components. Observer gain matrix G is designed such that the error dynamics are asymptotically stable with sufficient response. The dynamic behavior of the error vector is determined by the eigenvalues of the matrix $(A + G + E)$. If the eigenvalues of the matrix $(A + G + E)$ are chosen in such a way that the dynamic behavior of the error vector is asymptotically stable and is adequately fast, the error vector will tend to zero with adequate speed [19]. According to (2.a) and (2.b) in

 n information: DOI 10.1109/TMECH.2018.2817246, IEEE/ASME

Appendix A, adaptive algorithms are satisfied through PI controllers. Thus, the error of the MRAS current estimator is given as

$$e = \begin{bmatrix} i_q - \hat{i}_q \\ i_d - \hat{i}_d \end{bmatrix} \tag{11}$$

where the errors $i_q - \hat{i}_q$ and $i_d - \hat{i}_d$ are adjusted with the help of PI regulator coefficients according to the Popov's inequality criteria. Therefore, two error component parameters are given as [16]

$$\begin{aligned} \int_0^t [(i_d - \hat{i}_d)\frac{-i_d}{L_d} + (i_q - \hat{i}_q)\frac{-i_q}{L_q}]\left(R_s - \widehat{R}_s\right) dt \\ + \ [(i_q - \hat{i}_q)\omega_e]\,(\lambda_f - \hat{\lambda}_f)\, dt \\ \geq -{\gamma_0}^2 \end{aligned} \tag{12}$$

where ${\gamma_0}^2$ is a positive constant. When (9) and (10) are solved collectively, the error correction can be written as

$$\begin{aligned} \dot{e} = \begin{bmatrix} \dfrac{d(i_q - \hat{i}_q)}{dt} \\ \dfrac{d(i_d - \hat{i}_d)}{dt} \end{bmatrix} = \\ \left(\begin{bmatrix} -\dfrac{R_s}{L_q} & -\dfrac{L_d}{L_q}\omega_e \\ \dfrac{L_q}{L_d}\omega_e & -\dfrac{R_s}{L_d} \end{bmatrix} + \begin{bmatrix} G_1 & 0 \\ 0 & G_2 \end{bmatrix} \right) \begin{bmatrix} i_q - \hat{i}_q \\ i_d - \hat{i}_d \end{bmatrix} \\ + \left(\begin{bmatrix} -\dfrac{R_s}{L_q} & -\dfrac{L_d}{L_q}\omega_e \\ \dfrac{L_q}{L_d}\omega_e & -\dfrac{R_s}{L_d} \end{bmatrix} - \begin{bmatrix} -\dfrac{\widehat{R}_s}{L_q} & -\dfrac{L_d}{L_q}\omega_e \\ \dfrac{L_q}{L_d}\omega_e & -\dfrac{\widehat{R}_s}{L_d} \end{bmatrix} \right) \begin{bmatrix} \hat{i}_q \\ \hat{i}_d \end{bmatrix} \\ + \left(\begin{bmatrix} -\dfrac{\lambda_f}{L_q}\omega_e \\ 0 \end{bmatrix} - \begin{bmatrix} -\dfrac{\hat{\lambda}_f}{L_q}\omega_e \\ 0 \end{bmatrix} \right). \end{aligned} \tag{13}$$

Error correction is accomplished by an adaptation model. It is obtained by solving the nonlinear and feedforward linear model together in which $\hat{A} - A$ and $\hat{C} - C$ are used to obtain the reference and estimated currents that are the outputs of the estimation and reference models. Adaptation equations for $\widehat{R}_s$ and $\hat{\lambda}_f$ are given respectively as

$$\begin{aligned} \widehat{R}_s = -(k_{p_{res}} + \frac{k_{i_{res}}}{s})(L_s \hat{i}_d (i_d - \hat{i}_d) \\ + \hat{i}_q (i_q - \hat{i}_q)) + \widehat{R}_{s0} \end{aligned} \tag{14}$$

$$\hat{\lambda}_f = -\left(k_{p_{flux}} + \frac{k_{i_{flux}}}{s}\right)\omega_e (i_q - \hat{i}_q) L_s + \hat{\lambda}_{f0} \tag{15}$$

where $k_{p_{res}}$, $k_{i_{res}}$, $k_{p_{flux}}$, $k_{i_{flux}}$, $\widehat{R}_{s0}$, $\hat{\lambda}_{f0}$ are the proportional regulator coefficient of the estimated resistance, the integrator regulator coefficient of the estimated resistance, the proportional regulator coefficient of the estimated rotor flux linkage, the integrator regulator coefficient of the rotor flux linkage, and the initial estimated stator resistance and rotor flux linkage, respectively. Stator resistance and rotor flux linkage estimation values in (14) and (15) are guaranteed to provide faster response than the closed loop cycle. Since large state errors are constantly growing during the estimation period, selection of proper regulator parameters is crucial to minimize the steady-state error [17].

In the proposed MRAS method, a low-pass filter (LPF) is used to overcome the rise of the estimated rotor flux linkage value at low speed and at zero crossing and mitigates distortion effects caused from stator resistance estimation. At low speed where a LPF is not used, the estimation values are small and cause faulty feedforward voltage estimation values [44].

III. Stability Analysis

In this section, stability analysis is performed for the proposed sensorless PMSM drive scheme with MRAS parameter observer. In order to obtain the desired objectives, Modulus Optimum (MO) and Symmetrical Optimum (SO) tuning techniques for the complete model including delay elements, dq motor model, feedforward decoupling and MRAS parameter estimator structure are used to obtained the gains for the current and speed controllers, respectively. First, the inner current PI regulator gains and then the outer speed PI regulator gains are obtained with the desired settling time and overshoot using MO and SO techniques, respectively. The obtained PI regulator gains are used to construct the open and closed loop system transfer functions and then the stability analyses are performed accordingly for current and speed loops for various conditions including speed and parameter variations under full load.

A. Stability Analysis of the d– and q–axes Current Controllers

First, the open loop transfer function of the d–axis current loop is obtained without the PI controller, then the zero of the d–axis current PI controller is used to cancel out the largest time constant of the open-loop transfer function. That way MO design rules are confirmed for the d–axis current control. The stability analysis of the d–axis PI current controller is carried out in Matlab using the Bode plot. The d–axis current control results are obtained at 63 r/min speed under full load with and without parameter detuning. In detuned condition, the stator resistance is increased 30% higher than the rated value and rotor flux linkage is decreased by 20% of its rated value. The open-loop d–axis current control is a 17th-order system. The Bode plot for open loop d–axis current controller is shown in Fig. 4. The Gain Margin (GM) is 18.5 dB and the Phase Margin (PM) is 88.3 degrees for non-detuned parameters. In detuned parameter case, GM is 18.8 dB and PM is 98.7 degrees. In both cases, the system for closed-loop is stable.

Similar analysis is performed for the q–axis current loop. The open-loop Bode plot for the q–axis current controller is illustrated in Fig. 5. It is a 15th-order system. The Gain Margin (GM) is 20.4 dB and the Phase Margin (PM) is 103 degrees for non-detuned parameters. In detuned parameter case, GM is 20.7 dB and PM is 122 degrees. From the frequency domain stability criteria, in both cases, q–axis current control is stable.

n information: DOI 10.1109/TMECH.2018.2817246, IEEE/ASME

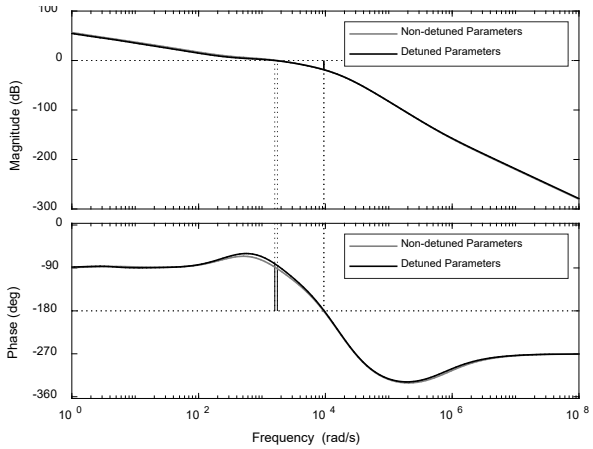

Fig. 4. Bode plot of the d–axis current control for detuned and non-detuned parameter conditions.

B. Stability Analysis of the Sensorless Speed Controller

In the open loop speed control transfer function, SO tuning technique is performed such that the combined small time constant pole is canceled out with the zero of the PI controller. As a result, at least one of the poles of the open loop speed transfer function resides at the origin itself or close to it, and the phase margin is maximized allowing more delays in the system. The stability analysis for the sensorless speed controller is performed at low speed (63 r/min) under full load for detuned and non-detuned parameter conditions using Bode plot and pole-zero map.

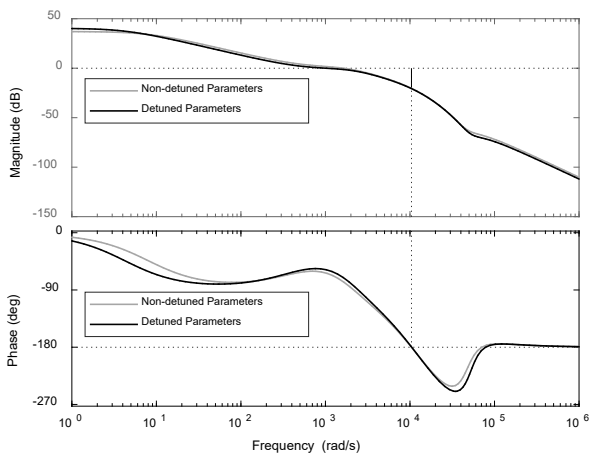

Fig. 5. Bode plot of the q–axis current control for detuned and non-detuned parameter conditions.

The open-loop Bode plot for the speed controller is illustrated in Fig. 6. At low frequency, phase does not change more than 180 degrees within the band of interest, therefore checking The Gain Margin (GM) for both detuned and non-detuned parameters is not necessary. In non-detuned and detuned parameter cases, Phase Margin (PM) is 80.9 degrees and 81.6 degrees, respectively. Therefore, frequency domain analysis of the speed closed loop system is stable.

The pole-zero map of the closed loop speed transfer function is shown in Fig. 7 for detuned and non-detuned parameter conditions. The close-up view of the dominant poles are illustrated in Fig. 8. The closed-loop speed control is a 17th-order system that has five complex conjugate poles in which two of them are cancelled with corresponding zeros. It is observed from the closed-loop sensorless speed transfer function, out of 17 poles three of them are located at zero as expected from the Symmetrical Optimum tuning method. The design of the speed controller parameters is selected to ensure that all of the poles and zeros are located in the Left Half Plane (LHP) of the $j\omega$–axis. In summary, the roots of the speed closed-loop in Fig. 7 show stable operation even for multi-parameter detuned conditions under full load in low speed region.

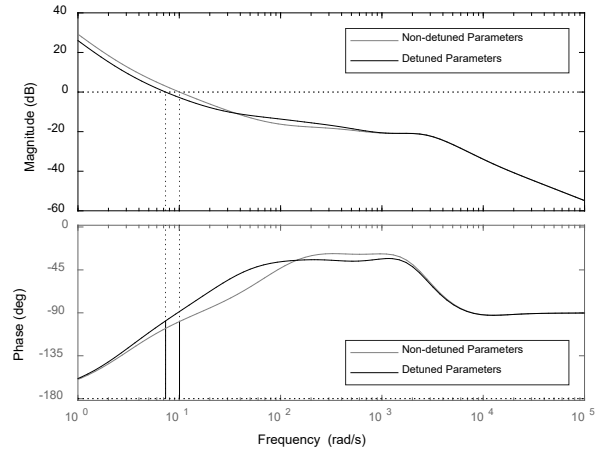

Fig. 6. Bode plot of the speed control loop for detuned and non-detuned parameter conditions.

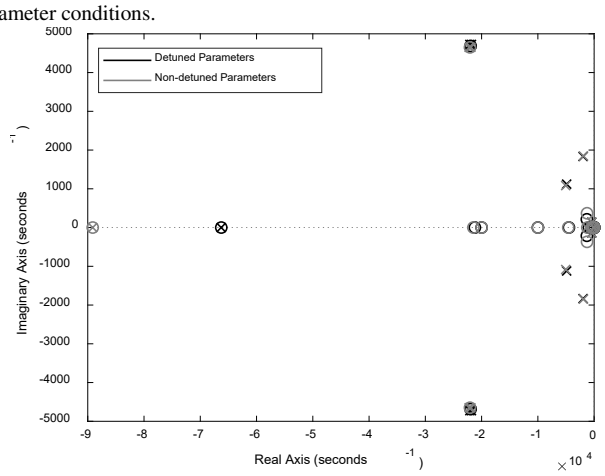

Fig. 7. Pole-zero map of the speed control loop for detuned and non-detuned parameter conditions.

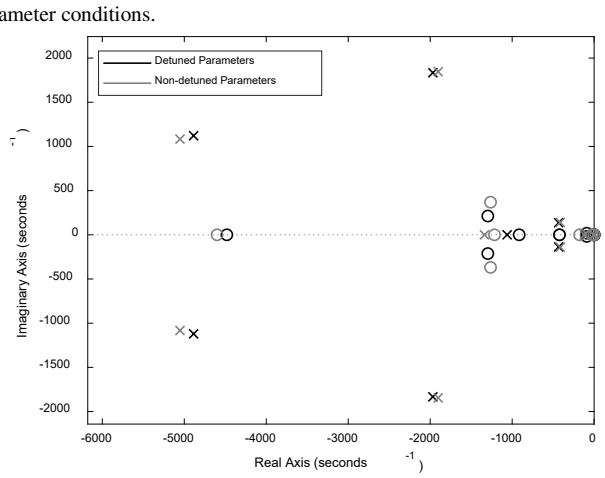

Fig. 8. Pole-zero map of the speed control loop for detuned and non-detuned parameter conditions (zoomed).

n information: DOI 10.1109/TMECH.2018.2817246, IEEE/ASME

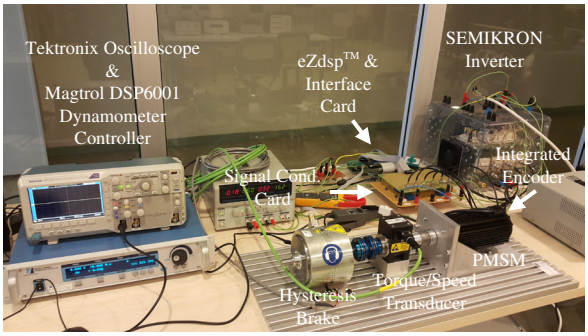

Fig. 9. Experimental test-bed.

IV. Experimental Results

The experimental set-up consists of a Magtrol AHB-6 model hysteresis dynamometer set, a SEMIKRON Semiteach inverter, a PM synchronous motor, an eZdsp™ board with TMS320F28335 DSP chip, and an interface and a signal conditioning cards. The proposed sensorless control scheme is verified using an off-the-shelf 2 N·m surface-mounted PMSM drive which is coupled to the overall system, as shown in Fig. 9. The system and control parameters are given in Appendix B in which the control parameters are provided in discrete-domain for per-unit system. The parameters and specifications of the PMSM are provided in Appendix C.

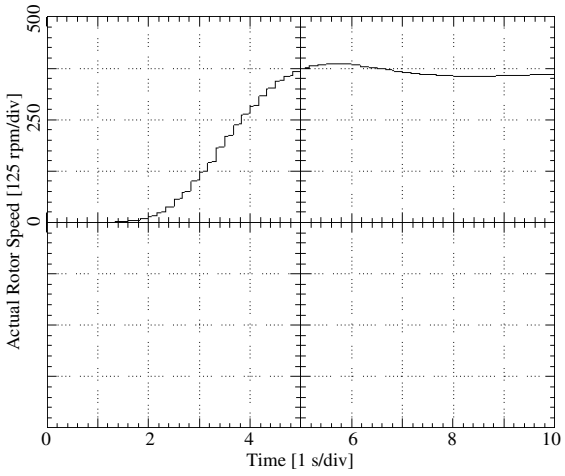

Fig. 10. Experimental rotor speed waveform under no load start-up without parameter estimation.

Fig. 10 shows the start-up performance of the proposed control method. No unstable state is observed at experimental no-load start-up using the proposed sensorless scheme, as shown in Fig. 10. Without estimation of parameters, results of load rejection and load injection of PMSM under 2 N·m full load as well as half full load rejection are shown in Fig. 11(a). At $t = 0$ s, PMSM is started with no load. During the steady-state under full-load at $t = 4$ s, sudden full load rejection of 2 N·m is applied using hysteresis brake which is set to zero. The proposed sensorless scheme has provided the stability of 360 r/min motor speed with desired response time. At $t = 11.2$ s, load injection is performed and the acceptable response of PMSM against sudden change of load is achieved. It is also seen in Fig. 11(a) that when half load rejection is applied at $t = 70$ s, the transient state as well as steady-state stability are still attained.

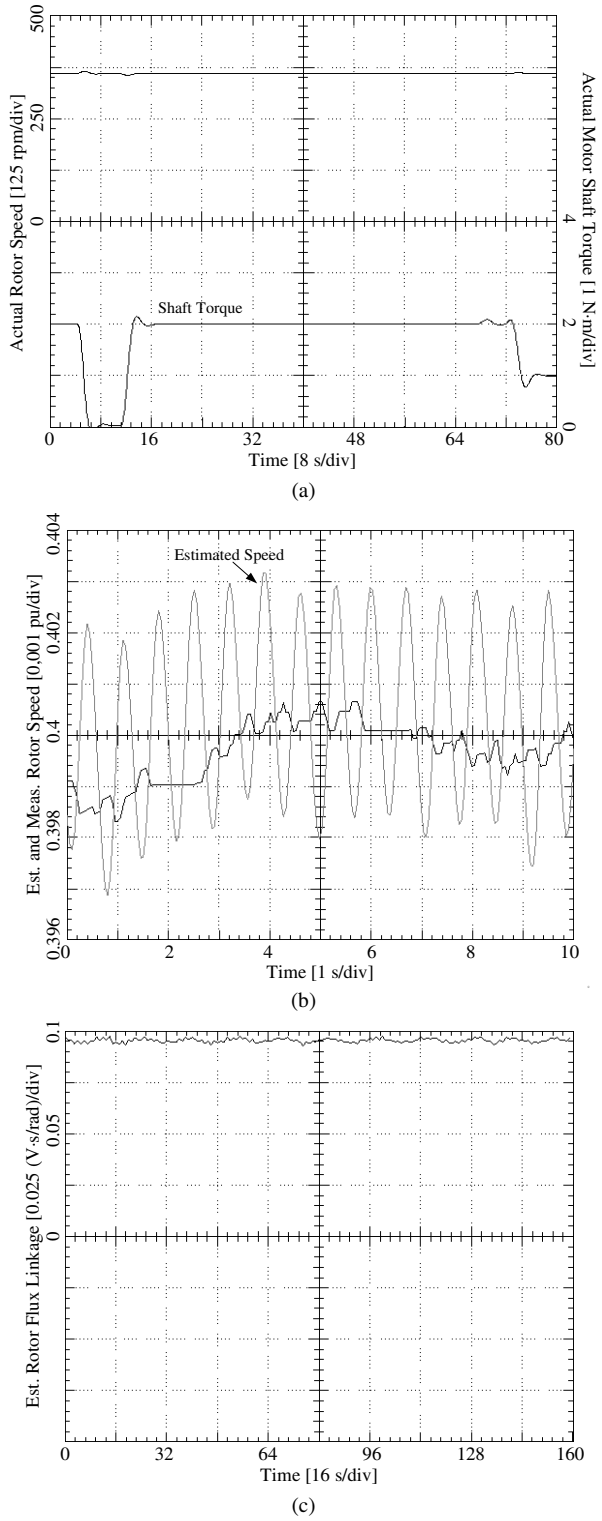

Fig. 11. (a) Experimental speed response when full load rejection (2 N·m) is employed at $t = 4$ s, full load injection is employed at $t = 11.2$ s, and half load rejection is applied at $t = 70$ s under 360 r/min steady-state speed without parameter estimation. (b) Experimental estimated and measured steady-state rotor speeds (360 r/min = 0.4 pu is the reference speed) under full-load. (c) Experimental estimated rotor flux linkage ($\lambda_{f(t=0)}$ = 0.0987 Vs/rad and the average estimated value is 0.09681 Vs/rad).

n information: DOI 10.1109/TMECH.2018.2817246, IEEE/ASME

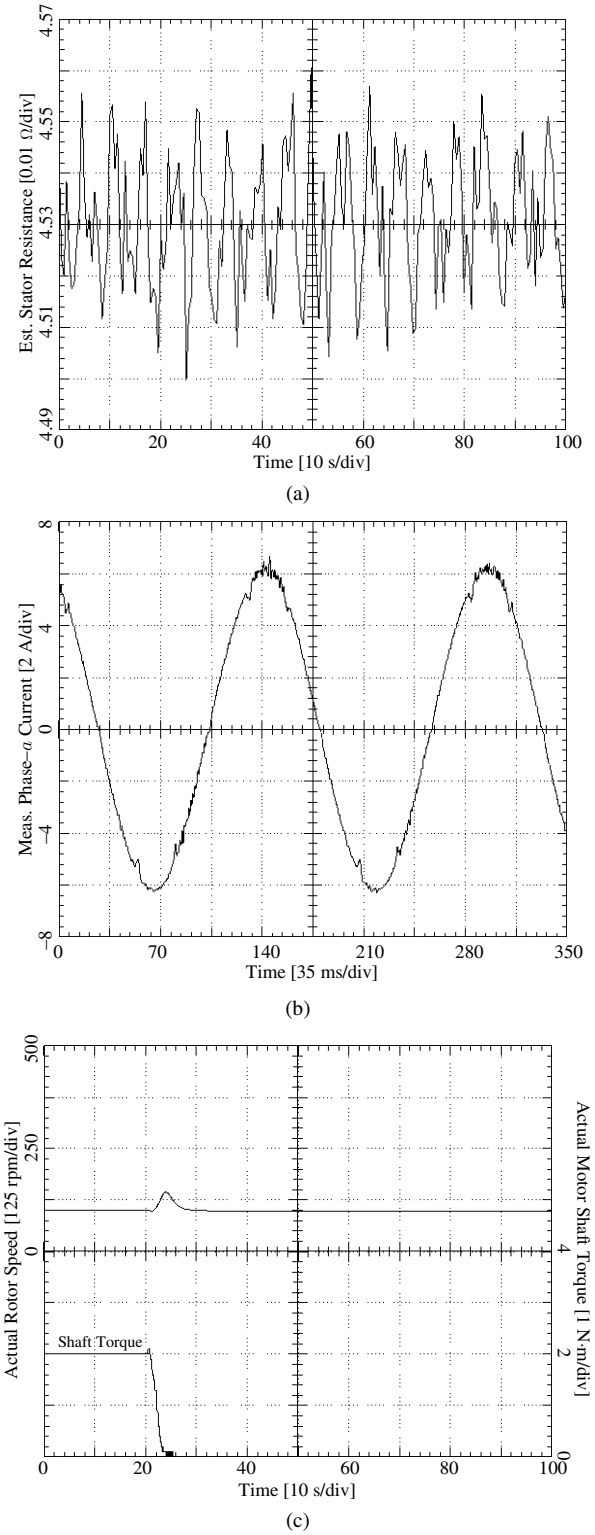

Fig. 12. (a) Experimental estimated stator resistance under 30% higher R_s. (b) Experimental steady-state phase–a current waveform under full load (2 N·m) with parameter estimation under 30% higher R_s. (Peak current value is 6.7 A). (c) Experimental rotor speed waveform at steady-state (100 r/min) under continuous full load and full load rejection conditions with parameter estimation during 30% higher stator resistance than the actual value.

Fig. 11(b) shows the comparison of estimated speed and the speed measured from the encoder at steady-state under full-load. The speed measured from the encoder and the one estimated by the proposed FFVE method track the reference speed value of 0.4 pu (360 r/min). This result shows the successful operation of the sensorless control method at medium speeds as well as under sudden speed and load changes.

Initial rotor flux linkage variation is shown in Fig. 11(c). In the experimental study, since the rotor flux linkage changes slowly, after obtaining the actual initial values and regulating the related controller parameters, update of the rotor flux variable which is found in q–axis feedforward voltage estimation model is ensured. Because the rotor flux linkage cannot be measured, it is only estimated, as shown in Fig. 11(c). To prevent saturations, saturation limits are defined even for a short time, therefore surpassing these limit values is prevented. Additionally, external three-phase resistance is physically inserted to the actual motor terminals to increase the total motor resistance artificially.

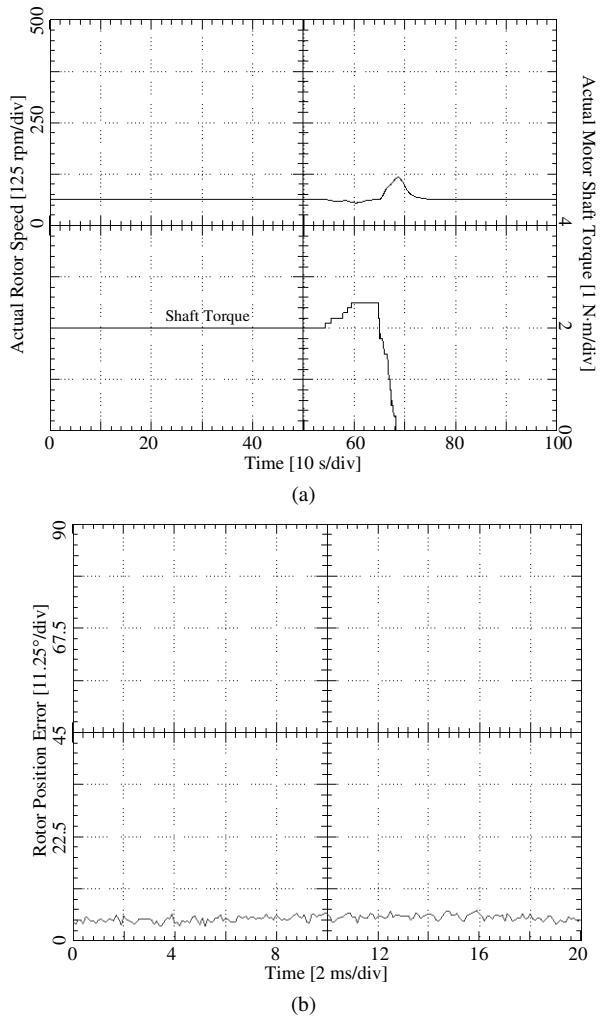

Fig. 13. (a) Experimental rotor speed waveform at steady-state (63 r/min) and transient when full load to no-load at $t = 55$ s is applied suddenly with parameter estimation during 30% higher stator resistance than the actual value. (b) Experimental mechanical rotor position error at steady-state (63 r/min) under full load condition with parameter estimation during 30% higher stator resistance than the actual value.

It is observed that the proposed sensorless control method without parameter estimation fails and loses stability when the motor is less than 240 r/min under full load. In contrast, the proposed system uses the estimated values of the stator resistance and rotor flux linkage to improve low speed perfor-

n information: DOI 10.1109/TMECH.2018.2817246, IEEE/ASME

mance. Fig. 12(a) illustrates the estimated steady-state stator resistance when the stator resistance is increased 30% from the rated value. Fig. 12(b) shows the phase–a current under 30% increased stator resistance. In this case, the peak value of the phase current is 6.7 A which is 18.5% higher than the nominal value under full-load. As shown in Fig. 12(c), since parameter variations are estimated in the low speed region, a stable operation is achieved at around 100 r/min. It is confirmed that the proposed sensorless drive system can operate even at 63 r/min under full load, as shown in Fig. 13(a). Fig. 13(b) shows the mechanical rotor position error when the motor speed is 63 r/min at steady-state under 30% higher stator resistance than the actual value under full-load.

The proposed control scheme is also compared with the well-known sensorless control method called sliding-mode speed observer (SMO). Sliding mode observer (SMO) is a promising approach for position sensorless schemes because of its independence to system parameter variations, fast convergence and robustness [45], [46]. First, the motor is brought up from zero speed to low speed at 100 r/min using open loop starting procedure under no-load. At that speed, the stator resistance is set to 130% of its actual value. Then, SMO is switched to achieve no-load closed-loop sensorless control. Then, the full-load is applied. From this point on, the data is started to be recorded, as shown in Fig. 14(a). Then, the full load is rejected at $t = 4$ s. At $t = 21.6$ s, full-load injection is applied. It is clear from Fig. 14(a) that the motor can follow the command speed with negligible overshoot and undershoot, speed ripple and without steady-state error at around 100 r/min under full load with classical SMO sensorless scheme. Fig. 14(b) illustrates the steady-state full-load phase–a current waveform obtained with classical SMO under 30% increased stator resistance. It is seen in Fig. 14(b) that the line current waveform using classical SMO shows similar results with the proposed control scheme under stable full-load operation. Due to the chattering effect, line current exhibits more ripples in the SMO case. Next, the rotor speed is attempted to be decreased more down to 63 r/min at $t = 5$ s during 30% higher stator resistance than the actual value as in the proposed scheme, however SMO cannot track the reference speed and the rotor speed starts to oscillate and eventually goes to zero, as seen in Fig. 14(c).

Moreover, the efficiency of the proposed control scheme has been compared to the classical SMO under same operating conditions. Since reactive power is minimized by proper stator d–axis voltage control in PMSM, it is expected from the FFVE which is based on stator voltage control and also immune to parameter variation, effective reactive power control is reached. The proposed method has 1.45% higher efficiency than the classical SMO under parameter variation.

The proposed control scheme which is capable of working at 4% lower speed compared to classical SMO, very low speed performance is limited compared to signal injection methods. The proposed method is quite practical in implementation compared to most of the sensorless methods. Although, the proposed sensorless method consists of several control loops, analysis shows that the total processing time is 0.5 μs shorter than the classical SMO.

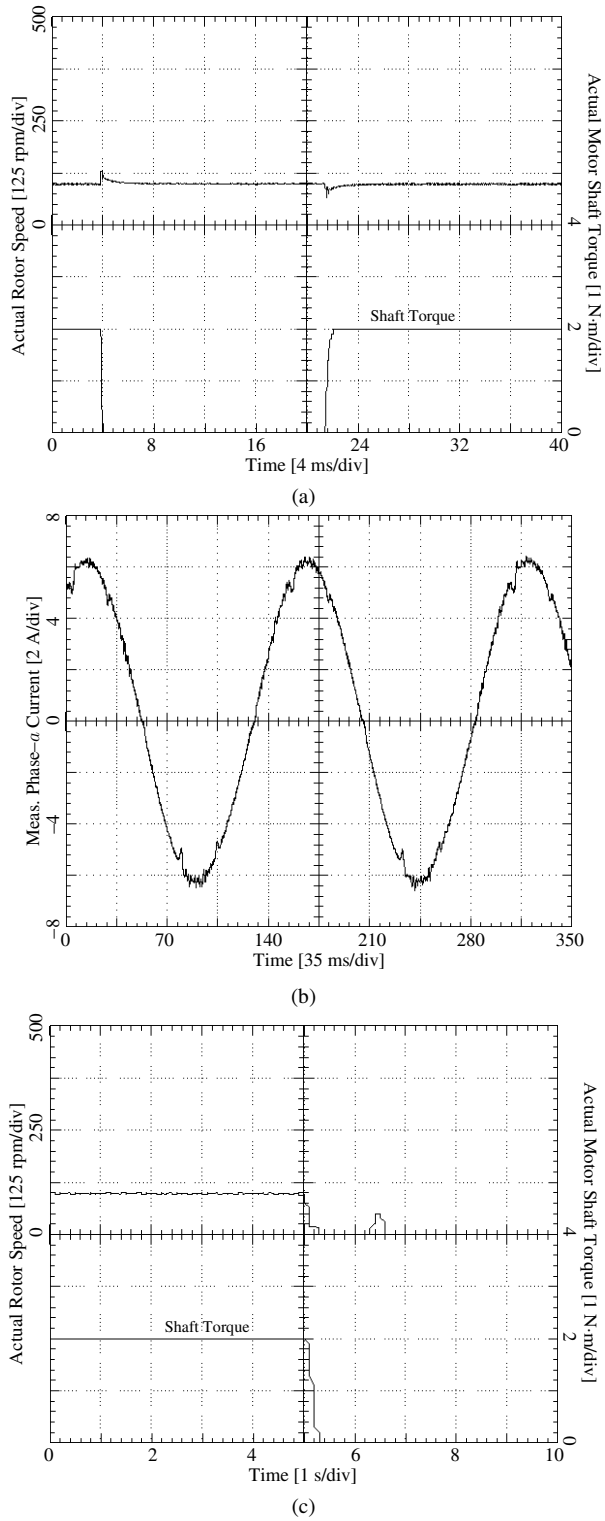

Fig. 14. (a) Experimental rotor speed waveform at steady-state (100 r/min) under continuous full load and full load rejection conditions during 30% higher stator resistance than the actual value using classical SMO. (b) Experimental steady-state full load (2 N·m) phase–a current waveform under 30% higher R_s using classical SMO. (c) Experimental rotor speed waveform at steady-state (100 r/min) and when the speed is stepped down to 63 r/min at $t = 5$ s during 30% higher stator resistance than the actual value using classical SMO.

The experimental results demonstrate that compared to the classical sliding-mode control (SMO), the proposed sensorless

 n information: DOI 10.1109/TMECH.2018.2817246, IEEE/ASME

method is stable at low speed ranges under full load even under heavy parameter detuning. Since the proposed method behaves like a V/f control as in induction motors, starting under no-load is possible as opposed to the classical back-EMF based sensorless methods such as sliding-mode in which starting under no-load is not feasible due to the lack of back-EMF information.

V. Conclusion

This paper presents a simple and dynamic position sensorless PMSM control method based on feedforward voltage estimation improved with a multi-parameter estimation method. The novelty of the proposed sensorless speed estimation technique lies with the fact that it is the first contribution to the literature regarding the stator feed-forward voltage estimation (FFVE) based sensorless control of PMSM drive that is insensitive to multi-parameter variations improved with model reference adaptive system (MRAS) under full load condition at low to nominal speed range. Compared to other sensorless methods, an easily implementable robust structure is proposed. Since the sensorless method is based on back-EMF estimation, the possible disturbance effects due to parameter changes are prevented with online MRAS multi-parameter estimation. Since the MRAS is easier to develop compared to other parameter estimation methods and due to the fact that the microprocessor is not overburdened, it is used in conjunction with feedforward voltage estimation. Therefore, in experimental studies, simultaneous estimation of both stator resistance and rotor flux linkage are ensured. Moreover, it is observed in the experiments that the proposed FFVE sensorless method which is similar to V/f control as in induction motors allows zero speed start-up to be possible and maintains stability at medium and nominal speeds under full-load. It also maintains the stability at low speeds down to 63 r/min under full-load when used with MRAS multi-parameter estimation under heavy parameter detuning.

Acknowledgment

This work was supported by The Scientific and Technological Research Council of Turkey (TUBITAK) funded project (112E263).

Appendix A

The proposed MRAS estimator is hyperstable, if the following two criterions are satisfied according to Popov's theorem,

1) The transfer function matrix of the linear forward block $[sI-(A+G+E)]^{-1}$ must be real and strictly positive.
2) The non-linear feedback block that satisfies Popov's criterion of,

$$\int_0^t W^T e dt \geq -\gamma_0{}^2 \tag{A.1}$$

where $t \geq 0$ [18].

Summing up $\dot{e} = (A+G)i_{\left[\substack{q\\d}\right]} + \Delta A\hat{i}_{\left[\substack{q\\d}\right]} + \Delta d + E.$ and (A.1) yields the following inequlities

(a) $\int_0^t e^T \Delta A\hat{i}_{\left[\substack{q\\d}\right]} dt \geq -\gamma_1{}^2$ for stator resistance estimation,

(b) $\int_0^t e^T \Delta d\ dt \geq -\gamma_2{}^2$ for rotor flux linkage estimation

where γ_0, γ_1, and γ_2 are a finite positive real constants, which are independent of t [18].

Appendix B

System and Control Parameters (per-unit)

Base frequency (Hz)	60
Switching frequency (kHz)	10
Sampling time (μs)	100
DC-link voltage (V)	565
Integral time constant for current (s)	9.706e-4
Proportional gain for current	0.4970
Integral gain for current	512.0784
Integral time constant for speed (s)	0.1238
Proportional gain for speed	0.2657
Integral gain for speed	2.1468
Speed feedback time constant (s)	0.009
Current feedback time constant (s)	5e-5
Feedforward gain	2.75
Sliding control gain	0.055
Sliding control filter coefficient	0.1

Appendix C

Parameters and Specifications of the PMSM

Number of poles	8
Line-to-neutral rms voltage (V)	230
Rated speed (r/min)	900
Rated rms current (A)	4
Rated torque (N·m)	2
Stator inductance (mH)	0.0033
Stator resistance (Ω)	3.4
Rotor magnetic flux linkage (Vs/rad)	0.0987
Moment of inertia (kg.m^2)	0.0075

References

[1] F. Aghili, "Energy-efficient and fault-tolerant control of multiphase nonsinusoidal pm synchronous machines," *IEEE/ASME Trans. Mechatronics*, vol. 20, no. 6, pp. 2736–2751, Dec. 2015.

[2] T. D. Do, H. H. Choi, and J.-W. Jung, "Nonlinear optimal DTC design and stability analysis for interior permanent magnet synchronous motor drives," *IEEE/ASME Trans. Mechatronics*, vol. 20, no. 6, pp. 2716–2725, Dec. 2015.

[3] X. Zhang and G. H. B. Foo, "A constant switching frequency-based direct torque control method for interior permanent-magnet synchronous motor drives," *IEEE/ASME Trans. Mechatronics*, vol. 21, no. 3, pp. 1445–1456, Jun. 2016.

[4] J.-K. Seok, J.-K. Lee, and D.-C. Lee, "Sensorless speed control of nonsalient permanent-magnet synchronous motor using rotor-position-tracking PI controller," *IEEE Trans. Ind. Electron.*, vol. 53, no. 2, pp. 399–405, Apr. 2006.

[5] T.-S. Low, T.-H. Lee, and K.-T. Chang, "A nonlinear speed observer for permanent-magnet synchronous motors," *IEEE Trans. Ind. Electron.*, vol. 40, no. 3, pp. 307–316, Jun. 1993.

[6] B. Stumberger, G. Stumberger, D. Dolinar, A. Hamler, and M. Trlep, "Evaluation of saturation and cross-magnetization effects in interior permanent-magnet synchronous motor," *IEEE Trans. Ind. Appl.*, vol. 39, no. 5, pp. 1264–1271, Sep. 2003.

[7] Y. Shi, K. Sun, L. Huang, and Y. Li, "Online identification of permanent magnet flux based on extended Kalman filter for IPMSM drive with position sensorless control," *IEEE Trans. Ind. Electron.*, vol. 59, no. 11, pp. 4169–4178, Nov. 2012.

[8] F. Auger, M. Hilairet, J. M. Guerrero, E. Monmasson, T. Orlowska-Kowalska, and S. Katsura, "Industrial applications of the Kalman filter: A review," *IEEE Trans. Ind. Electron.*, vol. 60, no. 12, pp. 5458–5471, Dec. 2013.

 n information: DOI 10.1109/TMECH.2018.2817246, IEEE/ASME

[9] S. Morimoto, M. Sanada, and Y. Takeda, "Mechanical sensorless drives of IPMSM with online parameter identification," *IEEE Trans. Ind. Appl.*, vol. 42, no. 5, pp. 1241–1248, Sep. 2006.

[10] S. J. Underwood and I. Husain, "Online parameter estimation and adaptive control of permanent-magnet synchronous machines," *IEEE Trans. Ind. Electron.*, vol. 57, no. 7, pp. 2435–2443, Jul. 2010.

[11] K. Liu, Z.-Q. Zhu, and D. A. Stone, "Parameter estimation for condition monitoring of PMSM stator winding and rotor permanent magnets," *IEEE Trans. Ind. Electron.*, vol. 60, no. 12, pp. 5902–5913, Dec. 2013.

[12] X. Luo, A. Shen, W. Cao, and W. Rao, "Full order state observer of stator flux for permanent magnet synchronous motor based on parameter adaptive identification," in *Proc. IEEE ICIEA*, 2013, pp. 1456–1461.

[13] T. Chan, W. Wang, P. Borsje, Y. Wong, and S. Ho, "Sensorless permanent-magnet synchronous motor drive using a reduced-order rotor flux observer," *IET Electr. Power Appl.*, vol. 2, no. 2, pp. 88–98, Mar. 2008.

[14] D. P. Marcetic and S. N. Vukosavic, "Speed-sensorless AC drives with the rotor time constant parameter update," *IEEE Trans. Ind. Electron.*, vol. 54, no. 5, pp. 2618–2625, Oct. 2007.

[15] T. Boileau, B. Nahid-Mobarakeh, and F. Meibody-Tabar, "On-line identification of PMSM parameters: Model-reference vs EKF," in *Proc. IEEE IAS,* 5–9 Oct., 2008, pp. 1–8.

[16] M. Eskola and H. Tuusa, "Comparison of MRAS and novel simple method for position estimation in PMSM drives," in *Proc. IEEE PESC,* 15–19 Jun., 2003, vol. 2, pp. 550–555.

[17] W. Zhifu, T. Qizhi, and Z. Chengning, "Speed identification about PMSM with MRAS," in *Proc. IEEE IPEMC,* 17–20 May, 2009, pp. 1880–1884.

[18] K.-H. Kim, S.-K. Chung, G.-W. Moon, I.-C. Baik, and M.-J. Youn, "Parameter estimation and control for permanent magnet synchronous motor drive using model reference adaptive technique," in *Proc. IEEE IECON*, 1995, vol. 1, pp. 387–392.

[19] K.-H. Kim, "DSP-based Sequential Parameter Estimation of PWM Inverter-fed IPM Synchronous Machine for Auto-tuning Applications," *Int. J. of Control and Autom.* (*IJCA*), vol. 6, no. 2, pp. 195–204, Apr. 2013.

[20] Z.-H. Liu, H.-L. Wei, Q.-C. Zhong, K. Liu, X.-S. Xiao, and L.-H. Wu, "Parameter estimation for VSI-Fed PMSM based on a dynamic PSO with learning strategies," *IEEE Trans. Power Electron.*, vol. 32, no. 4, pp. 3154–3165, Apr. 2017.

[21] Z.-H. Liu, H.-L. Wei, Q.-C. Zhong, K. Liu, and X.-H. Li, "GPU Implementation of DPSO-RE Algorithm for Parameters Identification of Surface PMSM Considering VSI Nonlinearity," *IEEE Trans. Emerg. Sel. Topics Power Electron.*, vol. 5, no. 3, pp. 1334–1345, Sept. 2017.

[22] W. Deng, C. Xia, Y. Yan, Q. Geng, and T. Shi, "Online Multiparameter Identification of Surface-Mounted PMSM Considering Inverter Disturbance Voltage," *IEEE Trans. Energy Convers.*, vol. 32, no. 1, pp. 202–212, Mar. 2017.

[23] D. Q. Dang, M. S. Rafaq; H. H. Choi, and J. W. Jung, "Online Parameter Estimation Technique for Adaptive Control Applications of Interior PM Synchronous Motor Drives," *IEEE Trans. Ind. Electron.*, vol. 63, no. 3, pp. 1438–1449, Mar. 2016.

[24] M. A. Hamida and J. De Leon and A. Glumineau and R. Boisliveau, "An Adaptive Interconnected Observer for Sensorless Control of PM Synchronous Motors With Online Parameter Identification," *IEEE Trans. Ind. Electron.*, vol. 60, no. 2, pp. 739–748, Feb. 2013.

[25] K. Liu and Q. Zhang and J. Chen and Z. Q. Zhu and J. Zhang, "Online Multiparameter Estimation of Nonsalient-Pole PM Synchronous Machines With Temperature Variation Tracking," *IEEE Trans. Ind. Electron.*, vol. 58, no. 5, pp. 1776–1788, May 2011.

[26] Q. Liu and K. Hameyer, "A fast online full parameter estimation of a PMSM with sinusoidal signal injection," in *Proc. IEEE ECCE*, Sept., 2015, pp. 4091–4096.

[27] G. Feng and C. Lai and N. C. Kar, "A Novel Current Injection-Based Online Parameter Estimation Method for PMSMs Considering Magnetic Saturation," *IEEE Trans. Magn.*, vol. 52, no. 7, pp. 1–4, Jul. 2016.

[28] G. Feng and C. Lai and K. Mukherjee and N. C. Kar, "Current Injection-Based Online Parameter and VSI Nonlinearity Estimation for PMSM Drives Using Current and Voltage DC Components," *IEEE Trans. Transport. Electrific.*, vol. 2, no. 2, pp. 119–128, Jun. 2016.

[29] H. S. Che, A. S. Abdel-Khalik, O. Dordevic, and E. Levi, "Parameter Estimation of Asymmetrical Six-phase Induction Machines using Modified Standard Tests," *IEEE Trans. Ind. Electron.*, vol. 64, no. 8, pp. 6075–6085, Aug. 2017.

[30] S. Yin, H. Yang, and O. Kaynak, "Sliding Mode Observer-Based FTC for Markovian Jump Systems with Actuator and Sensor Faults," *IEEE Trans. Autom.Control*, vol. 62, no. 7, pp. 3551–3558, Jul. 2017.

[31] J. Na, M. N. Mahyuddin, G. Herrmann, X. Ren, and P. Barber, "Robust adaptive finite-time parameter estimation and control for robotic systems," *Int. J. Robust Nonlinear Control*, vol. 25, no. 16, pp. 3045–3071, Nov. 2015.

[32] S. Yin, H. Gao, J. Qiu, and O. Kaynak, "Descriptor reduced-order sliding mode observers design for switched systems with sensor and actuator faults," *Automatica*, vol. 76, pp. 282–292, Feb. 2017.

[33] T. Okuyama, N. Fujimoto, T. Matsui, and Y. Kubota, "A high performance speed control scheme for induction motor without speed and voltage sensors," in *Conf. Rec. IEEE-IAS*, 1986, pp. 106–111.

[34] T. Okuyama, N. Fujimoto, T. Matsui, and Y. Kubota, "Vector control scheme of induction motor without speed and voltage sensors," *IEEJ Trans. Ind. Appl.*, vol. 107, no. 2, pp. 191–198, Feb. 1987.

[35] K. Nagata, T. Okuyama, H. Nemoto, and T. Katayama, "A simple robust voltage control of high power sensorless induction motor drives with high start torque demand," *IEEE Trans. Ind. Appl.*, vol. 44, no. 2, pp. 604–611, Mar. 2008.

[36] R. J. Kerkman, B. J. Seibel, T. M. Rowan, and D. W. Schlegel, "A new flux and stator resistance identifier for AC drive systems," *IEEE Trans. Ind. Appl.*, vol. 32, no. 3, pp. 585–593, May 1996.

[37] R. J. Kerkman, G. L. Skibinski, and D. W. Schlegel, "AC drives: Year 2000 (Y2K) and beyond," in *Proc. IEEE APEC,* 14–18 Mar., 1999, vol. 1, pp. 28–39.

[38] V. Blasko, L. Arnedo, and D. Jiang, "An integral method combining V/Hz and vector control of permanent magnet motor," in *Proc. IEEE ECCE,* 14–18 Sep., 2014, pp. 4472–4477.

[39] O. Sandre-Hernandez, R. Morales-Caporal, J. Rangel-Magdaleno, H. Peregrina-Barreto, and J. N. Hernandez-Perez, "Parameter identification of PMSMs using experimental measurements and a PSO algorithm," *IEEE Trans. Instrum. Meas.*, vol. 64, no. 8, pp. 2146–2154, Aug. 2015.

[40] J. Holtz, "Speed estimation and sensorless control of AC drives," in *Proc. IEEE IECON*, 1993, pp. 649–654.

[41] J. Holtz, "Sensorless control of induction motor drives," *Proc. IEEE*, vol. 90, no. 8, pp. 1359–1394, Aug. 2002.

[42] S. N. Vukosavic and A. M. Stankovic, "Sensorless induction motor drive with a single DC-link current sensor and instantaneous active and reactive power feedback," *IEEE Trans. Ind. Electron.*, vol. 48, no. 1, pp. 195–204, 2001.

[43] S.-S. Perng, Y.-S. Lai, and C.-H. Liu, "Sensorless control for induction motor drives based on new speed identification scheme," in *Proc. IEEE PCC*, 1997, vol. 2, pp. 553–558.

[44] J. Yan, H. Lin, Y. Feng, X. Guo, Y. Huang, and Z. Zhu, "Improved sliding mode model reference adaptive system speed observer for fuzzy control of direct-drive permanent magnet synchronous generator wind power generation system," *IET Renewable Power Gener.*, vol. 7, no. 1, pp. 28–35, Jan. 2013.

[45] F. Parasiliti, R. Petrella, and M. Tursini, "Sensorless speed control of a PM synchronous motor by sliding mode observer," in *Proc. IEEE ISIE*, 1997, pp. 1106–1111.

[46] Z. Yan and V. Utkin, "Sliding mode observers for electric machines-an overview," in *Proc. IEEE-IECON*, 2002, vol. 3, pp. 1842–1847.